Clinical Imaging 54 (2019) 40–47

Contents lists available at ScienceDirect

Clinical Imaging

journal homepage: www.elsevier.com/locate/clinimag

Pediatric Radiology

Infantile myofibromatosis: review of imaging findings and emphasis on correlation between MRI and histopathological findings

Lena Naffaa[a,*], Ibrahim Khalifeh[b], Rida Salman[a], Malak Itani[c], Raya Saab[d], Aghiad Al-kutoubi[a]

[a] Diagnostic Radiology Department, American University of Beirut Medical Center, PO Box 11-0236, Riad El Solh, 1107 2020 Beirut, Lebanon
[b] Department of Pathology and Laboratory Medicine, American University of Beirut Medical Center, PO Box 11-0236, Riad El Solh, 1107 2020 Beirut, Lebanon
[c] Department of Radiology, University of Washington, 4245 Roosevelt Way NE, Seattle, WA 98105, USA
[d] Department of Pediatrics and Adolescent Medicine, American University of Beirut Medical Center, PO Box 11-0236, Riad El Solh, 1107 2020 Beirut, Lebanon

ARTICLE INFO

Keywords:
MR-imaging
Pediatrics
Myofibromatosis
Pathology

ABSTRACT

Background: Infantile myofibromatosis (IM) is the most common fibrous tumor of infancy. MRI is considered the gold standard in IM evaluation. Very little has been published about IM with histopathology correlation in the pediatric age.

Purpose: Describe imaging findings in IM and correlate MRI findings with histopathology.

Material and methods: Imaging findings of 17 patients with IM were retrospectively analyzed including CT, US and MRI. Signal characteristics on T1-, T2-weighted and STIR imaging, extent of T2-hyperintensity, degree & pattern of enhancement, diffusion restriction, location & margins, & involvement of adjacent structures were tabulated. Histopathology findings included cellularity, collagenization, myxoid changes, atypia, mitosis & microscopic invasion. Established grading scores were utilized.

Results: Relative to normal skeletal muscle, on T1-weighted imaging, 9 lesions had similar signal while the remaining had a mixture of iso & hypo intensity; whereas on T2-weighted and STIR imaging, all 12 lesions demonstrated a mixture of iso, hypo & hyperintensity. T2-hyperintensity was grade 2 in one, grade 3 in 8 & grade 4 in 3 lesions. Intensity of enhancement was grade 2 in one, grade 3 in 8 & grade 4 in 3 lesions. Enhancement was predominantly peripheral in all 12 lesions.

Extent of T2-hyperintensity & degree of enhancement corresponded to variable grades on histopathology. CT and US showed nonspecific findings.

Conclusion: On MRI, IM has a mixture of signal intensity with predominant hyperintense signal on T2W images. However various signal & enhancement features correlated poorly with specific histopathologic grades.

1. Introduction

Infantile myofibromatosis (IM) is the most common fibrous tumor of infancy [1]. It tends to involve the skin, bone, muscle, and viscera [2]. It was initially described by Stout in 1954 and termed congenital generalized fibromatosis [3]. In 1981, the tumor was renamed by Chung et al. to reflect its myofibroblastic characteristics [4]. In 2002, IM was classified by World Health Organization as a benign category of fibroblastic-myofibroblastic lesions [5]. It is usually non-metastasizing. A small subgroup, aggressive fibromatosis, demonstrates local invasiveness and tendency to recur after surgical excision [6,7]. The majority of cases are diagnosed before the age of 2 years however this entity also occurs in older children and adults [4,8–10]. The juvenile form tends to have a more heterogeneous picture and different histology and behavior compared to the adult counterpart with a more infiltrative pattern and higher recurrence rate [11]. IM presents in 3 clinical forms: solitary, multicentric and generalized [1,4,12].

The initial imaging studies frequently include CT and US. However due to its inherent superior soft tissue resolution, MRI is considered the gold standard imaging technique in the detailed evaluation of IM [9,10,13–17].

In radiology literature, reports related to MRI findings of fibromatosis with histopathology correlation have been published with the largest series combining pediatric and adult patients [9,10,16]. Very little has been published about IM with histopathology correlation in the pediatric age, mainly a few case reports and a single case series of 7 cases [13–15,17], many of which are based on the older classifications. We present a series of 17 pediatric patients with IM according to

* Corresponding author.
E-mail addresses: ln01@aub.edu.lb (L. Naffaa), ik08@aub.edu.lb (I. Khalifeh), rs160@aub.edu.lb (R. Salman), rs88@aub.edu.lb (R. Saab), mk00@aub.edu.lb (A. Al-kutoubi).

https://doi.org/10.1016/j.clinimag.2018.11.003
Received 10 July 2018; Received in revised form 1 November 2018; Accepted 5 November 2018

Table 1
CT findings.

Pt #	Sex	Age	Location at initial diagnosis	Margins	CECT, attenuation relative to normal skeletal muscle	Bone involvement
1	M	3y	left parapharyngeal space to subcutaneous soft tissues of left lower face and upper neck	mixed	iso and lower attenuation	yes, cortical irregularity to angle of left mandible
2	F	2y	right carotid space at base of the neck	well defined	iso and higher attenuation (peripheral enhancement)	none
3	M	15y	left ethmoid sinus	well defined	hypo and higher attenuatuion (peripheral enhancement)	yes, erosion of the medial wall of left orbit, planum sphenoidale and left lesser wing of the sphenoid
4	F	21y	left gluteal muscles	ill defined	iso and lower attenuation	none
5	M	5 m	right posterior chest wall	well defined	lower and higher attenuation (peripheral enhancement)	yes, cortical disruption of the ribs
			spleen	well defined	lower and higher attenuation (peripheral enhancement)	
6	F	5y	left parapharyngeal space to subcutaneous tissue of the face	ill defined	iso attenuation	yes, erosion of left mandible
7	M	18y	left supra and infraclavicular spaces	ill defined	iso attenuation	none
8	M	10 y	multiple scalp lesions	well defined	iso and lower attenuation	none
9	M	20y	left infraclavicular space, subpectoralis	well defined	iso and lower attenuation	none

CT: Computed tomography, CECT: Contrast-enhanced computed tomography, Pt #: patient number, M: male, F: female, y: years, m: months.

the most recent WHO classification with description of the findings on various imaging modalities and detailed analysis of MRI characteristics with histopathology correlation.

2. Methods

The pathology records in our institution were searched for cases with proven IM in the pediatric and juvenile age group diagnosed between January 1, 2010 and December 31, 2015. We chose the upper age cutoff of 21 years old as pediatric oncology practice at our institution includes patients up to that age. A total of 17 patients with age range from 2 months to 21 years were included; 12 male patients and 5 female patients. The clinical, pathological and imaging findings were reviewed.

The CT images were acquired on a 64-slice CT scanner (Siemens, München, Germany) and included studies with intravenous iodinated contrast administration. The US images (Philips, Amsterdam, Holland) were acquired including Doppler assessment. The MRI images were acquired on 1.5 Tesla magnets (Philips, Amsterdam, Holland). MRI image acquisition protocol included: Spin echo T1-weighted [TR 244-706/TE 7-18], fast spin echo T2-weighted [TR 2000-6000/TE 100-40], STIR [TR 7864/TE 64], DWI [TR 6188/TE 68] and T1-weighted following the intravenous administration of 0.2 cc/kg of Dotarem (0.5 mmol/ml Guerbet, France) with fat suppression. The field of view ranged from 13 to 53 cm, slice thickness from 3.5 to 6 mm and section gap from 0.3 to 1 mm.

Data collected included the imaging findings on different modalities: the appearance of the lesion, tissue density and enhancement pattern, as well as bone involvement in patients with available CT scans and echogenicity and vascularity findings on ultrasound examinations.

The findings on MRI in patients for whom complete MRI records were available, were reviewed by two experienced radiologists (LN 16 years and AK 35 years) certified by The American Board of Radiology and the Royal College of Radiologists with a mean of 25.5 years' experience. The imaging findings were finalized after a consensus agreement between the two readers. For lesions that were biopsied, correlation was made to the findings on histopathology.

Findings evaluated on MRI included: signal intensity on T1- and T2-weighted and STIR images compared to skeletal muscle, hyperintensity on T2 compared to fat, extent of hyperintensity on T2-weighted imaging by visual estimation and grading, intensity of enhancement post intravenous gadolinium administration with grading by visual inspection, pattern of enhancement (central or peripheral enhancement), primary location and margins of the lesion (well defined, infiltrative or mixed), as well as secondary involvement of bone, muscle and neurovascular bundle.

Grading of extent of hyperintensity on T2-weighted and grading of intensity of enhancement post intravenous gadolinium were performed by visual estimation utilizing a 0–4 scale. Grade 0 is none, grade 1 is < 25% involvement of the lesion, grade 2 is between 25 and 50%, grade 3 is between 50 and 75% and grade 4 is > 75% involvement of the lesion [14].

Histopathologic findings were evaluated by a same experienced musculoskeletal pathologist blinded to the MRI findings. Features noted for each case included cellularity, extent of collagenization, myxoid changes, cytological atypia, mitosis and microscopic invasion. A 4-tiered system was used to approximate a score for the first 2 variables as follows: score 1 is < 25% involvement of the pathologic specimen, score 2 is between 25 and 50%, score 3 is between 50 and 75% and grade 4 is > 75% involvement [14]. The presence or absence of myxoid changes was noted as a score of 1 or 0 respectively. Since these lesions are classified as benign, three features were noted for their absence (score of 0) or mild presence only (score of 1): mild atypia, rare mitosis (1 to 2 per 10 high power fields, HPF), and focal microinvasion.

Data entry and statistical analyses were performed using (SPSS, V.23, 2009, Chicago, IL, USA).

Table 2
MR findings.

Pt #	Sex	Age	Location	Margins	Size (cm)	SI on T1	SI on T2	Recurrence	BI	NI
1	M	3y	left parapharyngeal space to subcutaneous tissues of left face	well defined	3.5 × 3.6 × 3.8	iso & hypo	hyper, hypo & iso	no	yes	no
2	F	2y	right carotid space at base of the of neck	well defined	4.3 × 2.7 × 5.6	iso	hyper, hypo & iso	the available MRI study is after recurrence in the same region	no	yes
3	M	15y	left ethmoid air cells	well defined	5 × 4 × 5	iso	hyper, hypo & iso	no	yes	no
4	F	21y	left gluteal muscles	mixed	2.5 × 5.5 × 4.5	iso	hyper, hypo & iso	multicentric	no	yes
10	M	2 m	proximal right thigh, deep to rectus femoris	well defined	1 × 1.2 × 1.4	iso	hyper, hypo & iso	no	no	no
11	M	3 m	left latissimus dorsi, serratus anterior and subscapularis	ill defined	8 × 6 × 10	iso	hyper, hypo & iso	no	no	no
12	M	13y	left proximal posterior muscle compartment of the thigh	mixed	5.7 × 3.5 × 17.8	Iso & hypo	hyper, hypo & iso	distal left posterior thigh muscles	no	yes
13	M	14y	right subscapularis, teres major and latissimus dorsi	mixed	7 × 6 × 14	iso & hypo	hyper, hypo & iso	no	no	no
14	M	16y	plantar subcutaneous tissue of left foot	well defined	1.7 × 2.2 × 0.7	iso	hyper, hypo & iso	no	no	no
15	F	18y	right distal quadriceps muscle and tendon	well defined	2 × 3 × 6	iso	hyper, hypo & iso	right groin	no	no
16	F	10 m	left knee joint	well defined	3 × 3 × 4	iso	hyper, hypo & iso	no	no	no
17	M	23 m	right parotid gland	well defined	2.9 × 2.3 × 3.1	iso	hyper, hypo & iso	no	no	no

SI: Signal intensity, Pt #: Patient number, imaging, BI: bone involvement, NI: neurovascular involvement, M: male, F: female, y: years, m: months.

Ethical approval

The study was approved by the institutional review board of the American University of Beirut (Protocol Number RAD.AA.01). There was no requirement for informed consent as it was waived by the IRB.

3. Results

A total of 17 patients with histopathologic diagnosis of myofibromatosis were reviewed. Nine patients had CT scans (Table 1), 2 patients had US and 12 patients had MRI exams (Tables 2).

Only one patient (patient#5) in our series had generalized form versus 16 patients who had the solitary/multicentric form.

3.1. CT findings

On contrast-enhanced CT scan, 6 out of the 9 lesions (66.7%) were of density similar or lower than adjacent muscles while the remaining lesions demonstrated peripheral mild enhancement., Six were male and three were female with age range from 5 months to 21 years (Median age: 10 years). There was predominance to the head and neck region (6 out of 9 lesions). Lesions were predominantly superficial in location, 6 out of the 9 lesions (66.7%) or showed a combination of subcutaneous and deep location. Bone involvement including cortical irregularity or erosion was noted when the lesion was close to bony structures in 4 out of the 9 lesions (66.7%). Splenic involvement was noted in one patient (patient #5) illustrating the ability of this condition to involve the abdominal viscera. (Fig. 1).

3.2. US findings

Five lesions were evaluated by US in two male patients with age range from 5 months to 20 years (median age: 10 years). The lesions were generally well defined with mixed echogenicity and decreased vascularity on Doppler relative to normal skeletal muscle. The solid organ involvement was well illustrated. (Fig. 2).

3.3. MRI findings

In the 12 patients with histopathologic diagnosis of IM and completed MRI examinations at initial presentation, 8 were male and 4 were female with age range from 2 months to 21 years (Median age: 8 years). Tables 3 & 4 display the imaging and histopathology features of this cohort of 12 patients. (Figs. 3–6).

One out of the 12 patients (8.3%), patient #10, had multicentric disease at initial diagnosis, involving besides the biopsied right proximal thigh lesion, multiple other sites in the subcutaneous tissue of the chest wall and back and the right occipital bone. Three out of the 12 patients (25%) including patient #10 had recurrence on follow up examinations in different locations than at the time of initial diagnosis; one other patient had recurrence in the same location in the carotid space, which was the only available study (pt#2).

Eight lesions (66.7%) had peripheral location in the upper and lower limbs, 3 were deeply located in the head and neck (carotid space, ethmoid sinus and parotid gland) and one lesion extended from deep parapharyngeal space to subcutaneous planes of the face. In the extremities, 5 patients had primary location in the muscle and one patient had an intra-articular lesion in the knee joint.

Apart from the lesions with primary intramuscular location, none of the lesions showed secondary involvement of adjacent muscles. Three out of the 12 lesions (25%) showed neurovascular involvement; 2 lesions encasing the adjacent portion of sciatic nerve and one lesion encasing the ipsilateral common carotid artery. Secondary bony involvement including cortical irregularity or erosion was seen in 2 out of the 12 lesions (16.7%), one centered in the ethmoid sinus causing erosion in the medial wall of the left orbit, planum sphenoidale and lesser wing

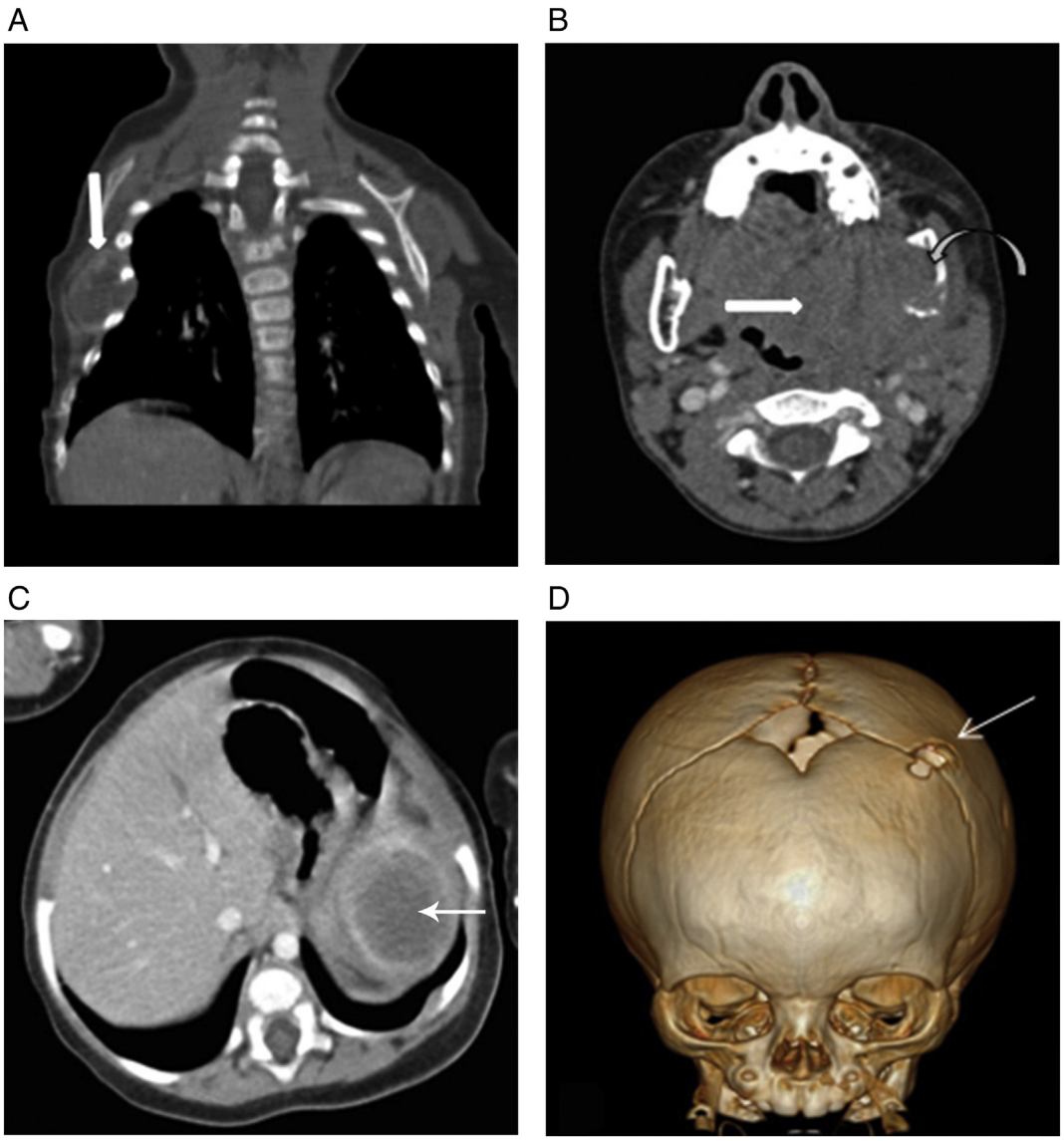

Fig. 1. CT images of IM: (A) Contrast enhanced coronal image of the chest in a 5-month-old boy with multi centric disease (patient#5). There is a right chest wall mass (Arrow) showing peripheral enhancement and causing deformity of the rib cage. (B) Contrast enhanced axial scan in a 5-year-old girl (patient#6) showing an ill-defined non-enhancing soft tissue mass (Arrow) extending from deep left parapharyngeal space where it impinges on the airways to the subcutaneous soft tissue of the neck. There is erosion of the left mandibular ramus (Curved arrow). (C) Contrast enhanced axial CT image in a 5-month-old boy (patient#5) demonstrating a circumscribed ovoid lesion in the spleen (Arrow) with peripheral wall enhancement and internal hypodensity. (D) 3D reconstruction of the skull demonstrating a lytic lesion (Arrow) in the left fronto-parietal bone crossing the suture line due to recurrence.

of the left sphenoid and the second in the left parapharyngeal space causing cortical irregularity as it passes behind the angle of the mandible to reach the face.

The maximum diameter of the masses as measured on MRI ranged from 1.4 cm to 17.8 cm.

The lesions had well defined margins in 8 out of the 12 (66.7%), infiltrative margins in 1 (8.3%) and mixed margins in the remaining 3 lesions (25%).

On T1-weighted imaging, 9 out of the 12 lesions (75%) had similar signal to normal skeletal muscle while the remaining lesions had a mixture of iso and hyposignal. On T2-weighted and STIR imaging, all 12 lesions demonstrated a mixture of iso, hypo and hyperintensity relative to normal skeletal muscle. The extent of hyperintensity of T2-weighted imaging was grade 2 in one lesion (8.3%), grade 3 in 8 (66.7%) and grade 4 in 3 lesions (25%). No lesion demonstrated fat-like signal. The intensity of enhancement was grade 2 in one out of the 12 lesions (8.3%), grade 3 in 8 lesions (66.7%) and grade 4 in 3 lesions (25%). Enhancement was heterogeneous and predominantly peripheral in all 12 lesions.

3.4. Histopathology findings

The histopathology findings were analyzed in the 12 patients with available MRI examinations as detailed in Tables 3 and 4.

In terms of hypercellularity, 4 out of 12 lesions (33.3%) were very hypercellular (S4), 6 (50%) were S3, and 2 (16.7%) were S2. The collagenization was S4 in 3 out of 12 lesions (25%), S3 in 3 (25%) and S2 in 6 (50%). Myxoid changes were only seen in 2 out of the 12 lesions (16.7%). Mitotic figures were only seen in 4 out of the 12 lesions (16.7%), reaching up to 1or 2 mitotic figures per 10 HPF. Mild atypia and focal microinvasion were not detected in any of the lesions. (Fig. 7).

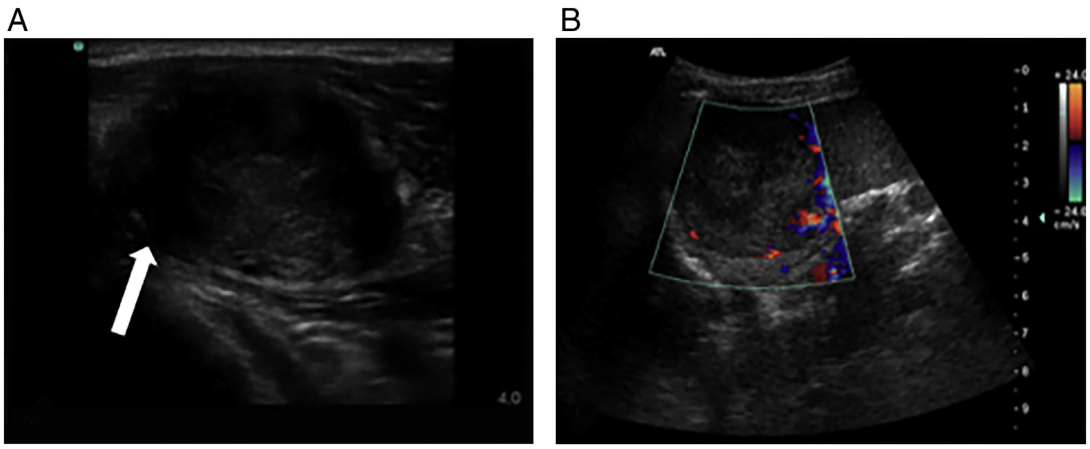

Fig. 2. US images of IM: (A) Transverse gray scale US image in a 20-year-old man (patient#9) showing a circumscribed subpectoralis ovoid lesion (Arrow) with mixed echogenicity, (B) Sagittal color-flow US image of a splenic lesion showing mild vascularity, mainly peripheral.

Table 3
T2 grading and histopathology findings.

		G2	G3	G4
Cellularity	S2	0	2	0
	S3	0	4	2
	S4	1	2	1
Collagenization	S2	0	4	2
	S3	1	2	0
	S4	0	2	1
Mixoid changes	0	0	7	3
	1	1	1	0
Mitosis	0	0	7	1
	1	1	1	2

Table 4
Enhancement grading and histopathology findings.

		G2	G3	G4
Cellularity	S2	0	2	0
	S3	0	4	2
	S4	1	2	1
Collagenization	S2	0	4	2
	S3	0	3	0
	S4	1	1	1
Mixoid changes	0	1	6	3
	1	0	2	0
Mitosis	0	1	6	1
	1	0	2	2

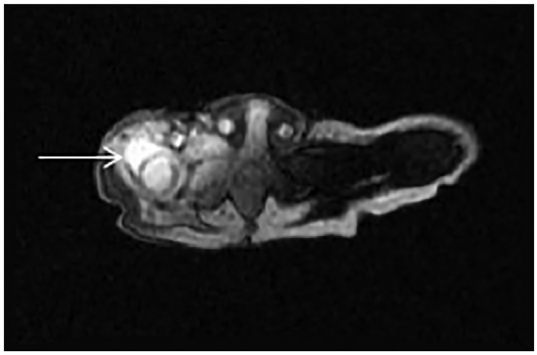

Fig. 3. MRI with Grade 4 enhancement: Axial T1-weighted image with fat saturation after intravenous gadolinium in a 2-month-old boy (patient#10) showing an intense G4 enhancement in the lesion at the right hip joint (Arrow).

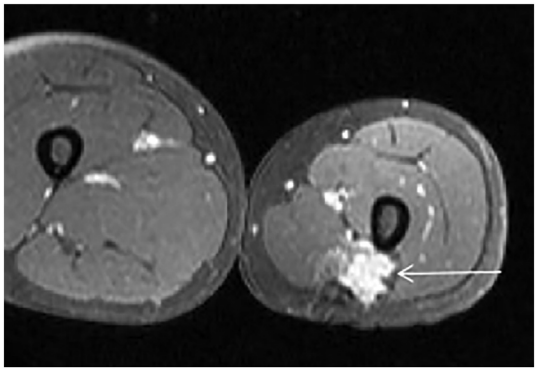

Fig. 4. MRI with Grade 3 enhancement: Axial T1-weighted image with fat saturation after iv gadolinium in a 13-year-old boy (patient#12) showing a G3 enhancement pattern more pronounced at the periphery of the lesion in the posterior aspect of the thigh (Arrow). Note the muscle atrophy on the side of the lesion.

3.5. MR and histopathology findings correlation

There is no statistical correlation between T2 grading and each histopathology finding; cellularity ($p = 0.758$), collagenization ($p = 0.682$), mixoid changes ($p = 0.212$) and mitosis ($p = 0.067$). There is also no statistical correlation between enhancement grading and each histopathology finding; cellularity ($p = 0.758$), collagenization ($p = 0.436$), mixoid changes ($p = 0.636$) and mitosis ($p = 0.661$). (Tables 3 and 4).

4. Discussion

IM has variable clinical presentations. The solitary form presents with subcutaneous erythematous nodules, the multicentric with subcutaneous, muscle and or bone lesions and the generalized form is a multicentric form with visceral involvement. The generalized form has the worst prognosis with a mortality rate approaching 15% [1]. The solitary form and multicentric form without visceral involvement generally have a good clinical outcome with a mortality rate of 1.3% and spontaneous regression of the lesions [1].

Despite its benign nature, IM may show insidious growth and sometimes aggressive characteristics hence the term aggressive fibromatosis or desmoids [15,18,19]. These latter lesions may infiltrate or encase adjacent structures like nerves, vessels, joints, or airways [15,18,19]. As imaging helps in defining their number, location, margins and involvement of adjacent structures, it is also essential in

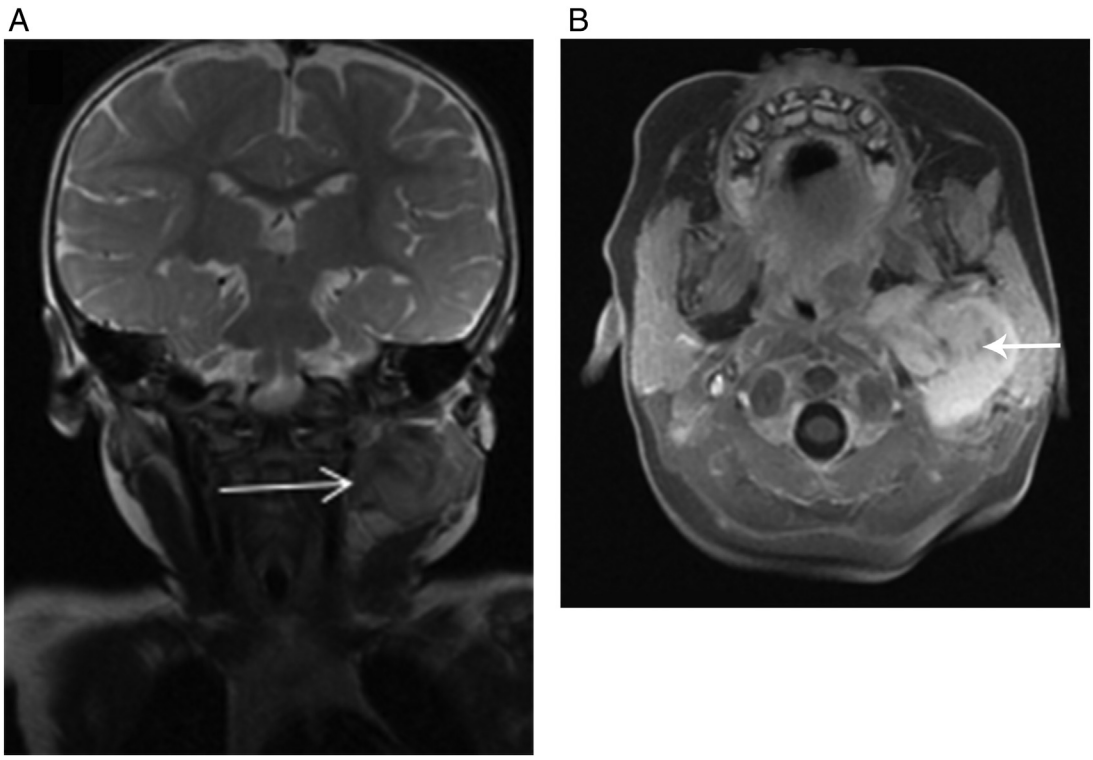

Fig. 5. MRI with Grade 3 enhancement: (A) Coronal T2-weighted image in a 3-year-old boy (patient#1) showing a well-defined left parapharyngeal mass (Arrow). The T2-hyperintensity relative to muscle is evident in about 65% of the lesion. (B) Axial post contrast T1-weighted image with fat saturation demonstrating a G3 enhancement pattern with subtle hypoenhancing internal foci (Arrow).

determining the feasibility of surgical resection and in delineating disease extent to help decide whether adjuvant chemotherapy is needed [15].

For palpable lesions, ultrasound is the first imaging modality due its lack of ionizing radiation and need for sedation and due to its easy availability and low cost. On Ultrasound, IM may have a variable

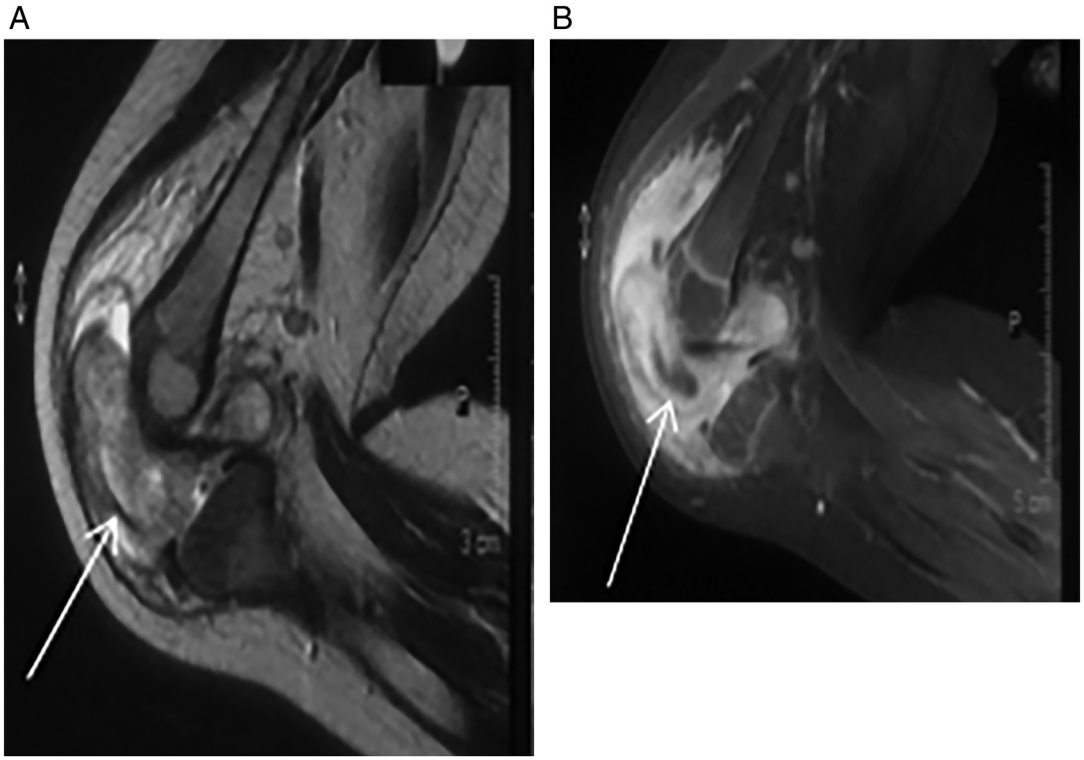

Fig. 6. MRI with grade 2 enhancement: (A) Sagittal T2-weighetd image showing a mixed signal mass within the knee joint (Arrow). (B) Sagittal fat saturation image after iv Gadolinium. There is approximately G2 enhancement in the mass (Arrow).

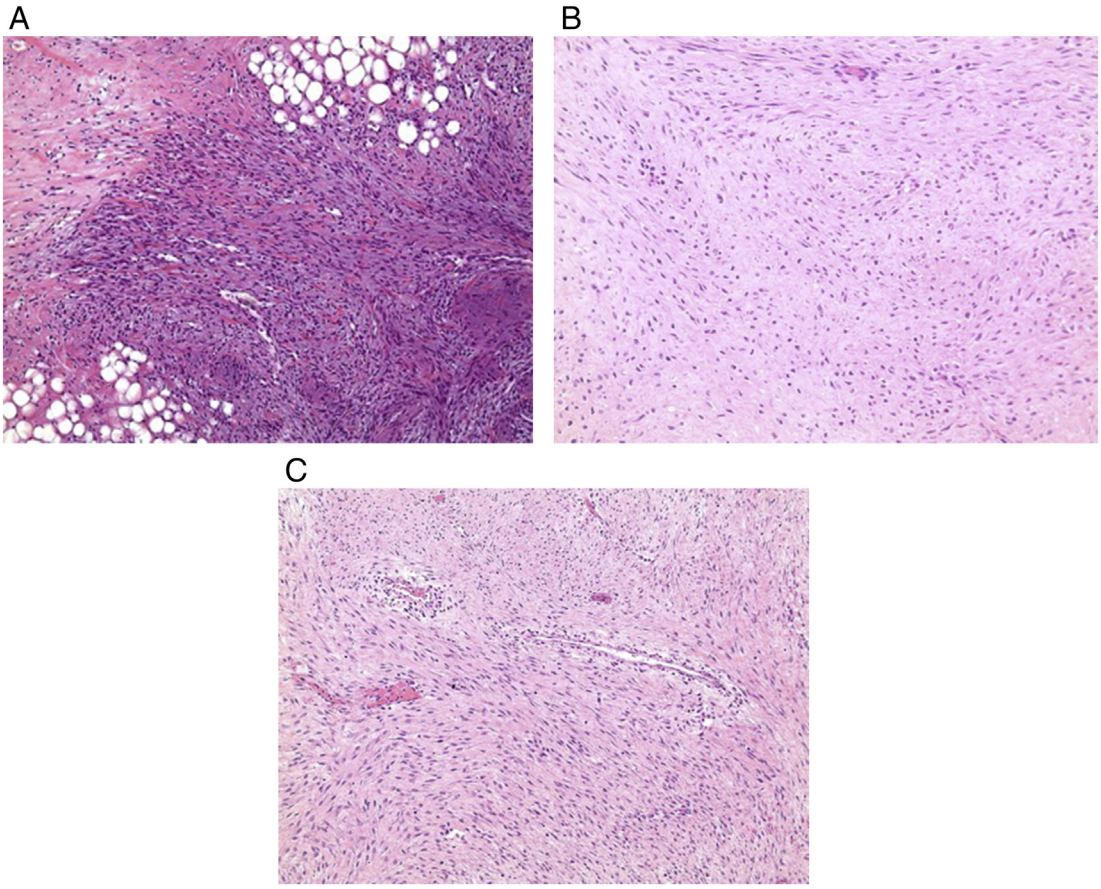

Fig. 7. Pathology examples: (A) Pathology slide from G4 enhancing lesion (Fig. 3) demonstrating elongated fibroblasts forming dense interlacing bundles with small amount of collagen. This lesion was characterized as S4 hypercellularity and S2 collagenization. (B) Light microscopic image of a G3 enhancing lesion (Fig. 4) showing a hypocellular proliferation of bland spindle cells forming elongated fascicles, S2. (C) Microscopic examination of a G3 enhancing mass (Fig. 5) showing mild cellularity (S2), and low collagen content (S2).

pattern and can be seen as a mass with a purely anechoic center and thick wall, a mass with a partially anechoic center, or a mass without anechoic component, and tend to be hypovascular on Doppler flow imaging [2]. Our ultrasound findings were comparable (Table 2, Fig. 2).

On CT, the appearance of IM is variable and nonspecific. With its limited spatial soft tissue resolution, CT has limited ability to evaluate the tumor margins and infiltration or encasement of surrounding structures. CT, however, has the advantage of more accurate assessment of bone involvement and destruction [15,20,21] which was found in 6 out of the 9 lesions with available CT scans when the lesion was close to bone structures (Table 1, Fig. 2&3). On enhanced CT, the masses have lower or similar attenuation compared to adjacent muscle, with some masses exhibiting peripheral enhancement [2], findings similar to our CT series (Table 1, Fig. 1). No consistent relationship has previously been found between the CT appearance of IM and their histology [22].

MRI is the gold standard technique to assess disease involvement of soft tissues [23]. The superior soft tissue resolution of MRI imaging and lack of beam-hardening artifacts adjacent to bone allow more accurate characterization, in particular assessment of infiltration of adjacent structures.

Whole-body MRI plays an important role in multicentric disease by its ability to detect the multiple soft tissue nodules characterized by myofibroblast proliferation. It provides a fast-complete imaging survey and allows thorough imaging of all lesions sized > 6 mm and the extent of disease and plays an important role in following up the evolution of those lesions [23–25].

On MRI, lesions may be well defined and nodular, or infiltrative and ill-defined [11,15]. Our results indicate variable tumor margins and could not predict microscopic invasion or cellular atypia similar to reports of Quinn et al. [9].

With regards to signal characteristics on MRI, Sundaram et al. in 1987 and Quinn et al. in 1991, analyzed the variable MRI signal characteristics of fibrous lesions and IM and concluded that the MRI appearance reflects differences in histologic composition i.e. cellularity, fibrous tissue content, and the presence of myxomatous degeneration rather than the histologic diagnosis [9,26]. On T1-weighted images, IM may be hypointense, isointense, of mixed intensity or rarely hyperintense relative to normal skeletal muscle whereas on T2-weighted images they tend to be of mixed signal intensity, predominantly hyperintense to muscle but hypointense to fat [9,14,15,26]. Comparison of T2-hyperintenisty relative to fat has been utilized for characterization of soft tissue masses, as increased T2 signal superior to that of fat may help differentiate malignant processes from desmoid tumors [10]. On the other hand, a low T2 signal, although rare, indicating a fibrous content was initially thought to differentiate desmoid tumors from malignant lesions [10], however this is no longer valuable as it can be seen in both [26]. Foci of low signal on both T1- and T2-weighted images are often seen, reflecting hypocellularity and abundant collagen [9,26]. Tumors with high cellularity and abundant collagen still show increased signal on T2-weighted images therefore the difference in T2-weighted signal appears to be determined by the degree of cellularity rather than the amount of collagen in the lesion [9,15,26]. Other investigators related the degree of hyperintensity of fibrous tumors on T2-weighted images to the stage of fibrosis, as more mature fibrosis tends to have more collagen fibers and less cellularity [13,27]. However, this finding was not consistently reproduced in the series of IM that were

evaluated by Ahn et al. in 2000 where the extent of hyperintensity on T2-weighted images did not correlate with the grade of cellularity, collagenization or myxoid changes probably because more than half of their patients had recurrent disease implying a less mature stage of fibrosis or because of MRI-sampling mismatch between area of hyperintensity and sampled specimen [14]. Our results in terms of extent of T2-hyperintensity indicate variable grades of cellularity, collagenization and myxoid changes (Table 4, Figs. 3–7) and therefore are concordant with the findings by Ahn et al. [14] and rather discordant with those of Quinn et al. [9]. The findings in our series cannot however be explained on the basis of recurrence and related immature fibrosis as in Ahn series, as only one of the 12 cohort of patients with MRI (pt#2) had biopsy of his recurrent disease in right carotid space.

The T2 and T1 signal characteristics of our lesions were comparable to other published series [14,20]. On T1-weighted images, a variable signal intensity was seen and on T2-weighted images, a combination of iso, hypo and hyperintense signal was encountered in all cases, with T2 signal intensity less than of fat favoring a benign lesion, findings that are also comparable to other reports by Ahn et al. and Eich et al. [14,20]. All lesions enhanced following intravenous contrast administration, showing heterogeneous enhancement with rather extensive enhancement in the grades 3 and 4 range which did not correlate to any specific histopathology grade. No correlation was found between the pattern of enhancement and tumor recurrence similar to the findings from Romero et al. [11].

Tumor size, extent of enhancement, and tumor margins correlated with variable grades cellularity, collagen deposition and myxoid changes similar to results from prior studies. No specific pattern was noticed in the cases which developed recurrence on follow-up exams (Table 2, pts #2, 12&15), in terms of pathologic grades, tumor size, margins of the lesions, extent of T2-hyperintensity or enhancement pattern.

Although limited data about the clinical outcome was available, no correlation or specific pattern is noted with MRI or histopathology findings (Tables 3 and 4). A larger sample is needed.

Eight subjects (66.7%) were followed up in a range of period between two and 14 years. Five out of eight subjects had recurrent disease (62.5%).

Our study suffers from limitations of small size and possible MR-pathology specimen mismatch. This latter factor is felt lessened as most of our lesions demonstrated a rather extensive hyperintensity on T2-weighted images (10 out of 12 were grades 3 and 4) and extensive enhancement post gadolinium administration (11 out of the 12 were grades 3 and 4). We advise future studies on this topic to be performed prospectively to be able to better control the sampling process.

Only one patient (patient#5) in our series had generalized form and this particular patient had no MRI at initial diagnosis, and therefore classifying our series into two sub-groups (generalized versus solitary/multicentric form) and further analysis could not be performed.

Another limitation is not performing statistical analysis about the inter-observer reliability between the two radiologists who finalized the imaging findings after a consensus agreement between them.

We believe that a specific point of strength of this study is that it includes the largest cohort of patients with correlation between the imaging and the most recent WHO pathology classification (2002).

In conclusion, the manifestations on imaging of myofibromatosis are variable and often nonspecific particularly on CT and US. A high index of suspicion for this condition in infancy and childhood should lead to the appropriate diagnosis and further assessment with MRI is warranted. On MRI, infantile myofibromatosis is predominantly a mass with peripheral enhancement showing a mixture of iso, hypo and hypersignal on T2-weighted images with T2 hypersignal being the most extensive component. Extent of enhancement and of T2-hyperintensity did not correlate with a specific histopathology grade. Tumor margins did not appear to predict microscopic invasion or atypia and the pattern of enhancement did not correlate with tumor recurrence.

CRediT authorship contribution statement

Lena Naffaa: Conceptualization, Formal analysis, Supervision, Writing - original draft, Writing - review & editing. **Ibrahim Khalifeh:** Formal analysis. **Rida Salman:** Data curation, Writing - review & editing. **Malak Itani:** Writing - review & editing. **Raya Saab:** Writing - review & editing. **Aghiad Al-kutoubi:** Conceptualization, Investigation, Writing - original draft, Writing - review & editing.

References

[1] Wiswell TE, Davis J, Cunningham BE, et al. Infantile myofibromatosis: the most common fibrous tumor of infancy. J Pediatr Surg 1988;2:315–8.
[2] Koujok K, Ruiz RE, Hernandez RJ. Myofibromatosis: imaging characteristics. Pediatr Radiol 2005;35:374–80.
[3] Stout AP. Juvenile fibromatosis. Cancer 1954;7:953–78.
[4] Chung EB, Enzinger FM. Infantile myofibromatosis. Cancer 1981;48:1807–18.
[5] Murphey MD, Ruble CM, Tyszko SM, et al. From the archives of the AFIP: musculoskeletal fibromatosis: radiologic-pathologic correlation. Radiographics 2009;29:2143–73.
[6] Feld R, Burk DL, McCue P, et al. MRI of aggressive fibromatosis: frequent appearance of high signal intensity on T2-weighted images. Magn. Reson. Imaging 1990;8:583–8.
[7] Soper JR, Silva MD. Infantile myofibromatosis: a radiological review. Pediatr Radiol 1993;23:189–94.
[8] Kacar A, Paker I, Orhan D, et al. Childhood fibroblastic and myofibroblastic tumors: a multicenter documentation and review of the literature. Turkish J. Pathol. 2012;28(1):24–30.
[9] Quinn SF, Erickson SJ, Dee PM, et al. MR imaging in fibromatosis: results in 26 patients with pathologic correlation. Am. J. Roentgenol. 1991 March;156:539–42.
[10] Hartman TE, Berquist TH, Fetsch JF. MR imaging of extraabdominal desmoids: differentiation from other neoplasms. Am. J. Roentgenol. 1992 March;158:581–5.
[11] Romero JA, Kim EE, Kim CG, et al. Different biologic features of desmoid tumors in adult and juvenile patients: MR demonstration. J Comput Assist Tomogr 1995 Sep-Oct;19(5):782–7.
[12] Oudijk L, Den Bakker MA, Hop WC, et al. Solitary, multifocal and generalized fibromas: clinicopathological and immunohistochemical features of 114 cases. Histopathology 2012;60:E1–11.
[13] Liu P, Thorner P. MRI of fibromatosis: with pathologic correlation. Pediatr Radiol 1992;22:587–9.
[14] Ahn JM, Yoon HK, Suh YL, et al. Infantile fibromatosis in childhood: findings on MR imaging and pathologic correlation. Clin Radiol 2000;55:19–24.
[15] Kingston CA, Owens CM, Jeanes A, et al. Imaging of desmoid fibromatosis in pediatric patients. Am. J. Roentgenol. 2002;178:191–9.
[16] Ya-Rong W, Wei W, Jia Z. Imaging features of aggressive fibromatosis in psoas muscle. J. Belge Radiol. 2011;94:283–6.
[17] Holzer-Fruehwald L, Blaser S, Rossi A, Fruehwald-Pallamar J. Imaging findings in seven cases of congenital infantile myofibromatosis with cerebral, spinal, or head and neck involvement. Neuroradiology 2012;54:1389–98.
[18] Enzinger FM, Weiss SW. Fibrous proliferations of infancy and childhood. In: Enzinger FM, Weiss SW, editors. Soft-Tissue Tumors. 3rd ed.St. Louis: Mosby; 1995. p. 231–68.
[19] Lewis JJ, Boland PJ, Leung DHY, et al. The enigma of desmoid tumors. Ann Surg 1999;229:866–73.
[20] Eich GF, Hoeffel JC, Tschappeler H, et al. Fibrous tumors in children: imaging features of a heterogenous group of disorders. Pediatr Radiol 1998;28:500–9.
[21] Johnson GL, Baisden BL, Fishman EK. Skeletal Radiol 1997 Oct;26(10):611–4.
[22] Francis IR, Dorovini-Zis K, Glazer GM, et al. The fibromatoses: CT-pathologic correlation. AJR Am. J. Roentgenol. 1986;147:1063–6.
[23] Counsel SJ, Devile C, Mercuri E, et al. Magnetic resonance imaging assessment of infantile myofibromatosis. Clin Radiol 2002;57:67–70.
[24] Chavhan GB, Babyn PS. Whole-body MR imaging in children: principles, technique, current applications and future directions radiographics. vol. 31. 2011. p. 1758–74.
[25] Teixeira SR, Elias Junior J, Nogueira-Barbosa MH, et al. Whole-body magnetic resonance imaging in children: state of the art. Radiol Bras 2015;48:111–20.
[26] Sundaram M, McGuire MH, Schajowicz F. Soft-tissue masses: histologic basis for decreased signal (short T2) on T2-weighted MR images. AJR Am J Roentgenol 1987;148:1247–50.
[27] Lee JKT, Galzer HS. Controversy in the MR imaging appearance of fibrosis. Radiology 1990:177–221.